Structure, Vol. 13, 131–141, January, 2005, ©2005 Elsevier Ltd All rights reserved. DOI 10.1016/j.str.2004.11.007

The "Roll and Lock" Mechanism of Force Generation in Muscle

Michael A. Ferenczi,[1,6,*] Sergey Y. Bershitsky,[2,6] Natalia Koubassova,[3,6] Verl Siththanandan,[1] William I. Helsby,[4] Pierre Panine,[5] Manfred Roessle,[5] Theyencheri Narayanan,[5] and Andrey K. Tsaturyan[3,6]

[1]Imperial College
London SW7 2AZ
United Kingdom

[2]Institute of Immunology and Physiology
Ural Branch
Russian Academy of Sciences
Yekaterinburg 620219
Russia

[3]Institute of Mechanics
Moscow University
Moscow 119992
Russia

[4]Daresbury Laboratory
Cheshire WA4 4AD
United Kingdom

[5]ESRF
BP 220
F-38043 Grenoble
France

Summary

Muscle force results from the interaction of the globular heads of myosin-II with actin filaments. We studied the structure-function relationship in the myosin motor in contracting muscle fibers by using temperature jumps or length steps combined with time-resolved, low-angle X-ray diffraction. Both perturbations induced simultaneous changes in the active muscle force and in the extent of labeling of the actin helix by stereo-specifically bound myosin heads at a constant total number of attached heads. The generally accepted hypothesis assumes that muscle force is generated solely by tilting of the lever arm, or the light chain domain of the myosin head, about its catalytic domain firmly bound to actin. Data obtained suggest an additional force-generating step: the "roll and lock" transition of catalytic domains of non-stereo-specifically attached heads to a stereo-specifically bound state. A model based on this scheme is described to quantitatively explain the data.

Introduction

The current lever arm hypothesis (Holmes, 1997) suggests that the actin-myosin motor in contracting vertebrate skeletal muscle produces force or displacement by a tilt of the light chain, or "neck," domain of the myosin head (myosin subfragment 1, or S1) with respect to its catalytic domain, which remains in a fixed position on actin. Crystallographic (Smith and Rayment, 1996; Houdusse et al., 1999, 2000), electron microscopy (Burgess et al., 2002), and spectroscopic data (Yasunaga et al., 2000; Forkey et al., 2003) support this hypothesis and show a nucleotide dependent 40°–75° tilt of the neck domain equivalent to an axial movement of the end of the lever arm of 5–12 nm in myosin-II. So far, all atomic S1 structures were obtained in the absence of actin. For this reason, the possible role of molecular interactions at the actin-S1 interface in force generation remains obscure. Nucleotide-induced changes in affinity of myosin heads for actin have been known for many years but remain unexplained at a molecular level. Recent crystallographic (Coureux et al., 2003; Reubold et al., 2003) data, results of docking of high-resolution crystallographic structures into low-resolution cryo-EM images (Volkmann et al., 2003; Holmes et al., 2003), and fluorescence measurements (Conibear et al., 2003) reveal conformational changes in the actin binding domain of S1. It is hypothesized that these changes are responsible for the transition from weak to strong binding of S1 to actin and are essential processes for the function of the myosin motor.

We previously reported results of experiments with frog muscle fibers in which we observed a concomitant increase in force and in the intensity, I_{A1}, of the first actin layer line, A1, at 1/37 nm^{-1} in the X-ray diffraction pattern when temperature increased, while fiber stiffness was unchanged (Bershitsky et al., 1997; Tsaturyan et al., 1999a). This was interpreted as an increase in the number of myosin heads stereo-specifically labeling the actin helix. EM-tomography of contracting insect flight muscles (Taylor et al., 1999) shows that myosin heads can have different orientations of their motor domains with respect to actin in contracting muscle. Despite this, the simplest assumption that during force generation the motor domain of S1 has a fixed position on actin and that the major moving part of the motor is the neck of S1 is commonly used (Irving et al., 2000; Piazzesi et al., 2002). A model calculation showed that I_{A1} is insensitive to a tilt of the lever arm if the catalytic domain remains in a fixed position on actin (Koubassova and Tsaturyan, 2002). This supports an involvement of a "locking" transition from a non-stereo-specific to a stereo-specific binding of S1 to actin in force generation (Bershitsky et al., 1997; Taylor et al., 1999; Tsaturyan et al., 1999a; Huxley, 2000; Kraft et al., 2002). The term "stereo-specific binding" implies a fixed position of the catalytic domain of S1 with respect to actin, so that its position in space is fully determined by the position of the actin monomer(s) it is bound to. "Non-stereo-specific binding" means that the actin-myosin interface has substantial axial stiffness but allows attachment of the catalytic domain of S1 to actin at different azimuthal and axial angles so that the contribution of myosin heads to the actin layer lines is low. Such non-stereo-specific binding probably takes place via electrostatic interactions (Rayment et al., 1993). Actin activation of the myosin ATPase and the affinity of S1 to actin depend on charges in loop 2 of S1 and in the

*Correspondence: m.ferenczi@imperial.ac.uk
[6]These authors contributed equally to the work.

subdomain 1 of actin but are not very sensitive to their position in the amino acid sequences (Furch et al., 1998; Wong et al., 1999; Joel et al., 2001). These findings, as well as the high variability in the length and amino acid sequence of loop 2 among myosins of the myosin-II subfamily (Cope et al., 1996), provide evidence that this electrostatic contact is not stereo-specific.

Here, we report the results of probing the structure-function relationship in muscle myosin-II by using temperature jump (T-jump) in contracting permeabilized fibers from rabbit muscle. T-jump and length step perturbations were used to synchronize force-generating events in myosin crossbridges. The response to, and relaxation from, these perturbations reveal intrinsic molecular processes in the muscle fiber which are those responsible for muscle contraction under physiological conditions. Structural changes were monitored with low-angle X-ray diffraction at 1 ms time resolution. The results strongly support our hypothesis (Bershitsky et al., 1997) that force generation is tightly coupled with a "locking" transition, irrespective of the type of perturbation used to synchronize the force-generating events. A new model in which force generation is a two-step process quantitatively explains the data. The first step is a "roll and lock" transition of non-stereo-specifically attached myosin heads to a stereo-specifically bound state. The second step is lever arm tilting. Both processes are coupled to different stages in the pathway of ATP hydrolysis, which is the source of energy for muscle contraction.

Results

Actin Labeling by Bound Myosin Heads during Low- and High-Tension Contraction

The T-jump from 5°C to 30°C in permeabilized fibers from rabbit muscle induced a 3-fold increase in active fiber tension. Changes in the 2D, low-angle X-ray diffraction pattern collected with a CCD X-ray detector during and after the tension rise are shown in Figure 1. Due to the relatively long read-out time of the CCD detector, only three time frames were recorded in this series of experiments: "cold" and "hot" steady-state frames on the plateau of contraction at pre- (5°C) and post-T-jump (30°C) temperatures and an "intermediate," 5 ms long period occurring half-way during the tension rise after the T-jump (Figure 2A). The difference between the "hot" and "cold" diffraction patterns revealed that the intensities of all actin layer lines from A1 to A7 increased with temperature in parallel with tension (Figures 1 and 2A). These layer lines originate from diffraction on the actin helix (~37 nm period). When myosin heads bind actin stereo-specifically, they adopt the symmetry of the actin helix so that the axial spacing of the layer lines remains the same as in the absence of bound myosin heads, but their intensities are higher. The intensities of the actin layer lines are determined by the number of myosin heads incorporated into the actin helix and by their conformation. The intensities of the actin-myosin beating layer lines AM_{-1} and AM_{+1} at 1/24 nm^{-1} and 1/10.4 nm^{-1}, respectively, also increased after the T-jump (Figure 1). These layer lines arise from axial modulation of the actin labeling pattern by myosin heads that occurs because myosin heads bound to an actin filament originate from the different crowns of myosin molecules separated axially by ~14.5 nm along the myosin filaments. These beating layer lines are specific indicators of binding of myosin heads to actin with myosin-based periodicity (Bordas et al., 1993; Yagi, 1996; Tsaturyan, 2002; Koubassova and Tsaturyan, 2002). In the "intermediate," frame the intensities of all actin- and actin-myosin-based layer lines were approximately half-way between their values in the "cold" and "hot" steady states (Figure 1), showing that the extent of labeling of the actin helix by stereo-specifically bound heads increases approximately proportionally to tension.

The intensity of the myosin meridional reflection M3, I_{M3}, at ~1/14.5 nm^{-1} in the "hot" frame was ~55% higher than that in the "cold" one (Figure 1). In the "intermediate," frame the M3 intensity was approximately the same as that in the "cold" frame (Figure 1), while the average tension was half-way between its pre- and post-T-jump steady-state levels (Figure 2A). The intensity of the M6 myosin meridional reflection at ~1/7.28 nm^{-1} decreased after the T-jump (Figure 1). In different sets of experiments, it was reduced by 15%–20% and 5%–15% in the "hot" and "intermediate" frames respectively, compared to the "cold" one.

In another set of experiments with the same three-frame protocol (Figure 2A) but with a longer camera (Figure 2B), the A1 actin layer line was clearly separated from the neighboring first myosin layer line M1 at 1/43.5 nm^{-1}. The latter arises from the axial period of helical origins of myosin heads on the thick filaments. While the A1 intensity increased 2.5 times with temperature, the M1 intensity changed by less than 10% (Figure 2B). As seen from Figure 2C, the temperature-dependent increase in the intensities of the A6 and A7 actin layer lines at ~1/5.9 nm^{-1} and ~1/5.1 nm^{-1}, respectively, in contracting muscle occurred at the same reciprocal radii as that at which myosin heads contribute to these intensities in rigor, i.e., in the absence of ATP when all myosin heads are strongly bound to actin. The changes in the intensity of the A6 and A7 layer lines were 9% and 7%, respectively, for the "intermediate" frame compared to the "cold" one. During the "hot" frame, the increases in these intensities were 15% and 17%, respectively, compared to the values at 5°C. The observed position of the peak on the A5 actin layer line reflection during contraction is closer to the meridian than in rigor (Figure 2C). This means that the configuration of myosin heads stereo-specifically bound to actin in contracting muscle is different from that in rigor. Results of the modeling of the intensity distribution along this layer line (Koubassova and Tsaturyan, 2002) show that the neck domains of the bound heads are more perpendicular to the filament axis due to a tilt or a bend compared to their rigor configuration observed by EM (Holmes et al., 2003). Changes in the diffraction pattern after the T-jump demonstrate that at higher temperature and tension the number of myosin heads incorporated into the actin helix increases and this process is probably essential for force generation in muscle.

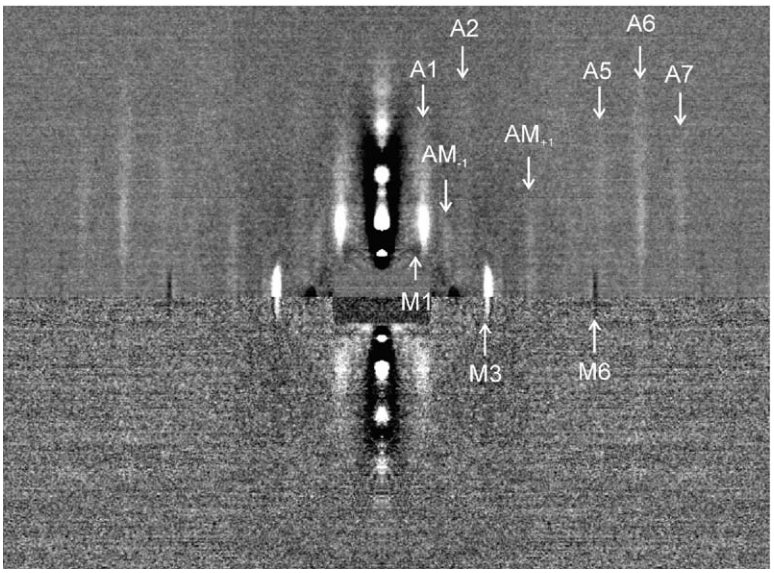

Figure 1. Changes in the 2D X-Ray Diffraction Pattern in the Three-Frame T-Jump Protocol

The differences between the diffraction patterns collected in the "hot" (30°C) and "cold" (5°C) frames (upper half) and between the "intermediate" and "cold" frames (lower half) are shown. The diffraction pattern collected during the 5 ms-long "cold" period was arithmetically subtracted from the 5 ms-long "hot" diffraction pattern pixel by pixel to obtain the difference pattern. The same procedure was used for the "intermediate" frame. Prior to subtraction, the intensities of the four quadrants were averaged in each frame. The timing of the frames in relation to the tension transient after the T-jump is shown in Figure 2A. The gray-scale indicates the magnitude of change in the intensity of X-ray diffraction, with the highest increase in intensity shown in white, and the largest decrease shown in black. The equator is vertical, and the position of some actin, myosin, and beating actin-myosin layer lines is labeled with arrows. Data were collected from 90 T-jumps in 5 bundles with a 2.5 m long camera, incident beam flux 10^{13} photons/s.

Time-Resolved Mechanical and Structural Changes Induced by T-Jumps

Figure 3 shows the averaged temperature and tension traces and the time course of I_{A1}, I_{M3}, and of the equatorial reflections (1,0) and (1,1) recorded at ESRF with the RAPID detector from five fiber bundles with 1 ms time resolution. During the T-jump, tension decreased slightly due to thermal expansion and then rose 3-fold (3.3 ± 0.2, mean ± SD here and elsewhere) with a half-time of 3.4 ms (range of 2.9–3.9 ms). The tension rise was not monoexponential. To compare it with the time courses of X-ray reflections, it was fitted with an exponential with an apparent rate constant of 188 ± 12 s^{-1}. When sarcomere length was recorded simultaneously, it remained constant (change of <2 nm per half sarcomere) for 5–6 ms after the T-jump and then slowly decreased (n = 3, Figure 3). I_{A1} increased 2.5-fold with an apparent rate constant of 235 ± 50 s^{-1} (Figure 3). In contrast, I_{M3} dropped by 20% during the 1 ms-long T-jump, remained low for the next 1 ms, and then increased to a level 60% higher than that before the T-jump with an apparent rate constant of 240 ± 18 s^{-1}, similar to that of tension and I_{A1}. Its intensity is sensitive to axial tilting of S1 or its neck domain (Irving et al., 1992, 2000; Dobbie et al., 1998). $I_{1,0}$, the intensity of the (1,0) equatorial reflection, decreased by 19% simultaneously with tension, while $I_{1,1}$, the intensity of the (1,1) reflection, was constant within 2% accuracy.

The time courses of changes in tension, I_{A1}, I_{M3}, and $I_{1,0}$ are shown in Figure 4. The initial decrease in I_{M3} was significantly faster than changes in tension, $I_{1,0}$, and I_{A1} and was similar to that observed in intact frog muscle fibers in responses to the length step changes (Irving et al., 1992, 2000). The subsequent rise of I_{M3} had the same apparent rate constant as that of $I_{1,0}$ and I_{A1}. Note that the fast initial change in I_{M3} was not accompanied by any simultaneous changes in tension (Figures 3 and 4). The difference in the time courses of tension and I_{M3} indicates that the tension rise after the T-jump is not controlled by a one-step process, but has a more complex nature.

Both I_{A1} and $I_{1,0}$ changed simultaneously with tension or even slightly faster. The temperature independence of fiber stiffness (Tsaturyan et al., 1999a; Bershitsky and

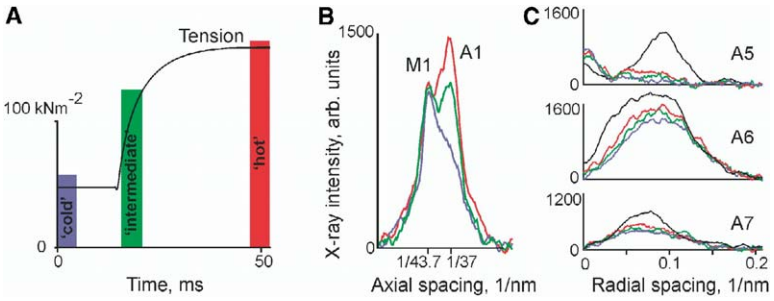

Figure 2. Changes in Tension and Intensity Distribution of Some Layer Lines in the Three-Frame T-Jump Protocol

(A) Average tension trace. Blue, green, and red bars on the tension trace show the timing of the "cold," "intermediate," and "hot" frames, respectively.

(B) The intensity of the M1 and A1 layer lines (flux 2.4 × 10^{13} photons/s, 77 T-jumps, 9 bundles, 10 m long camera). Radial integration was from 0.0269–0.091 nm^{-1}, with subtracted background intensity. The axial positions of the A1 and M1 layer lines in rigor and for relaxed fiber bundles are shown.

(C) Intensity profiles of the A5, A6, and A7 actin layer lines (same data set as in Figure 1). Rigor profiles collected from the same bundles are shown in black. Blue, green, and red lines in (B) and (C) correspond to the "cold," "intermediate," and "hot" frames, respectively.

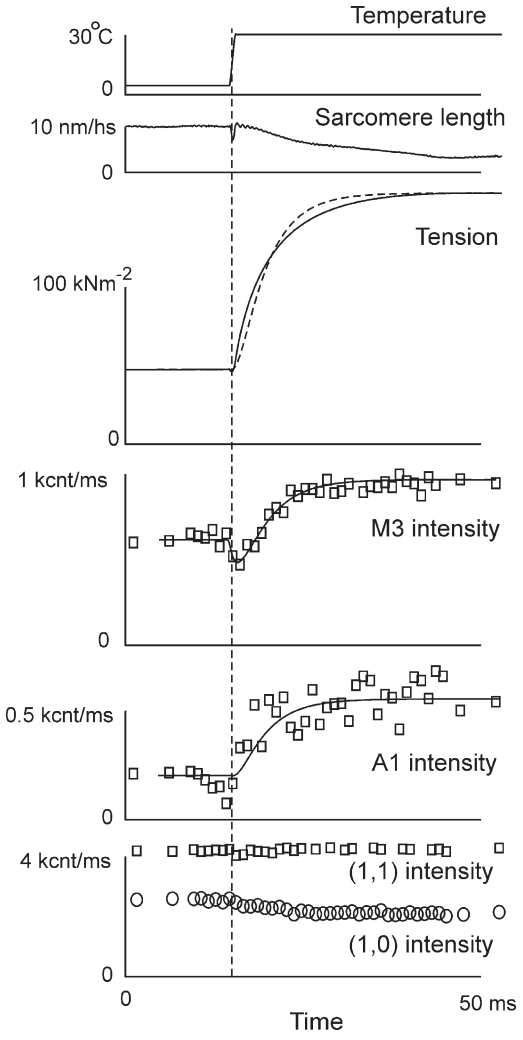

Figure 3. Time Course of Mechanical and Structural Responses to the T-Jumps

Top to bottom: averaged temperature, representative sarcomere length trace, averaged tension, I_{M3}, I_{A1}, and $I_{1,1}$ (squares), and $I_{1,0}$ (circles) collected from 150 T-jumps in 5 bundles, flux 10^{13} photons/s. X-ray intensities are expressed in kilocounts per 1 ms. The smooth lines superimposed with I_{M3} and I_{A1} data and the dashed line superimposed with the tension trace are the results of modeling (Figures 6 and 7). A vertical line marks the time when the T-jump was half complete.

Tsaturyan, 2002; Piazzesi et al., 2003) and of $I_{1,1}$ indicates that the number of myosin heads attached to actin does not change with temperature and that the increase in tension at higher temperature is caused by an increase in the average force produced by a myosin head. The significant increase in I_{A1} after the T-jumps must be caused by a "locking" of myosin heads on actin. This is because I_{A1} is independent of the tilting of the "lever arm" of the heads if their catalytic domains are stereo-specifically bound to actin. The contribution of non-stereo-specifically bound myosin heads to the actin layer line intensities is low because the distribution of their electron density in space does not follow a helical symmetry.

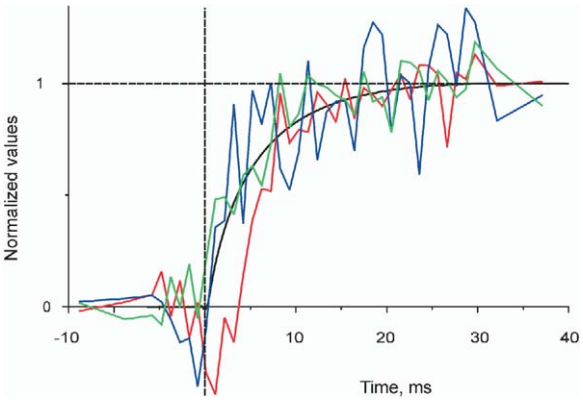

Figure 4. Normalized Time Course of Mechanical and Structural Responses to the T-Jumps

Normalized tension (black line), I_{A1} (blue line), $I_{1,0}$ (green line), and I_{M3} (red line) for the same data as in Figure 3. A vertical line marks the time when the T-jump was half complete.

Strain Dependence of Actin Labeling by Myosin Heads in Contracting Muscle

The simultaneous increase in tension and in I_{A1} after a T-jump demonstrates that a "locking" of myosin heads in a stereo-specifically bound state is an essential part of force generation. However, it is not clear whether this locking itself is accompanied by an axial tilt of the heads, leading to force generation, or alternatively whether a force-generating event takes place after the locking. To answer this question, we studied the mechanical and structural responses of contracting muscle fibers to step length changes and paid particular attention to the intensity of the brightest actin layer line, A1. If the locking is part of the force-generating transition(s), it should be accompanied by a "rolling" axial movement of the head. If this is the case, the locking must be strain dependent due to the contribution of elastic energy to the free energy of the transition (Huxley and Simmons, 1971). Therefore, shortening should facilitate the locking, while a stretch should hamper it, so that the number of myosin heads incorporated into the actin helix and thus I_{A1} should increase after a release and decrease after a stretch.

Figure 5 shows the results of time-resolved experiments carried out at the Daresbury Laboratory, where stretch-release cycles were applied to contracting bundles of permeabilized fibers from rabbit muscle. The amplitude of stretches and releases was ~5 nm per half-sarcomere, and the duration of the steps was 0.15 ms, with 5 ms intervals between stretches and releases (Figure 5A). Stretches induced a fast decrease in I_{M3} by ~35%, while releases recovered I_{M3}. Changes in I_{M3} begun during a 0.15 ms-long length step and finished about 1 ms after the end of the step (Figure 5A). The intensity in the region of the first actin/myosin layer line, LL1, also decreased by ~25% after the stretch and recovered after the release (Figure 5A). The data were too noisy to obtain submillisecond time resolution, but the changes were essentially complete in 1–2 ms after a length step, i.e., at the end of the Huxley-Simmons phase 2 (Figure 5A). The spatial resolution was insufficient for decomposing the intensity into the

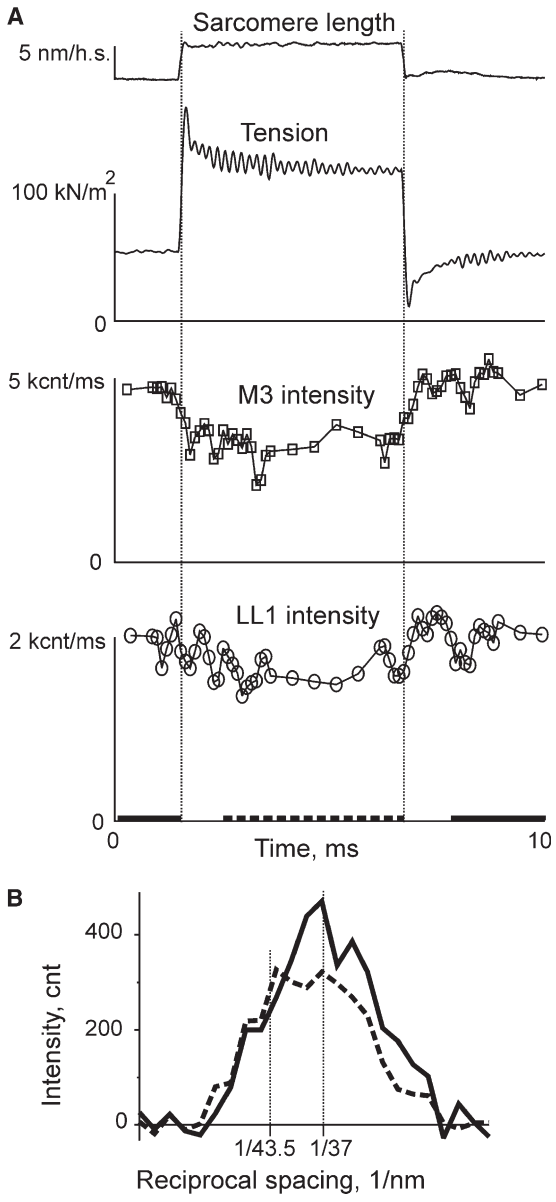

Figure 5. Results of the Length Step Experiments

(A) Top to bottom: a representative sarcomere length record, averaged tension response, the intensities (in kilocounts per 1 ms) of the M3 myosin meridional reflection and of the first actin/myosin layer line (LL1). Data from four bundles of rabbit muscle fibers on beam line 16.1. 7,000 stretch-release cycles with a 10 ms period (5 ms between the length steps) were applied to each bundle with acquisition time frames for the X-ray data of 0.1 ms and 0.5 ms. The vertical dotted lines mark the times when the length steps were half complete.

(B) Intensity profiles in the region of the first actin and the first myosin layer lines (radial integration from 0.0267–0.0656 nm^{-1}, background intensity subtracted) during 4 ms time intervals before releases and stretches in each cycle. The time intervals when the pre-stretch (solid line) and pre-release (dashed line) intensities were collected are shown in Figure 5A by the horizontal solid and dashed lines, respectively. The meridional spacing of A1, 1/37 nm^{-1}, and of M1, 1/43.5 nm^{-1}, in rigor and relaxed states, respectively, are shown as references.

M1 and A1 components. To be sure that the changes observed were indeed associated with A1, the intensity in the region of the layer lines was integrated in the radial direction during 4 ms-long periods immediately before releases and stretches when the intensity of the layer line was constant (Figure 5A). No significant difference in the intensity was found in the M1 region (Figure 5B). All observed changes in the intensity of this complex layer line were seen at an axial spacing corresponding to the A1 position so that I_{A1} changed by ~30% (Figure 5B). The model of Koubassova and Tsaturyan (2002) shows that changes in I_{A1}, which can be induced by an axial and/or azimuthal tilt of the light chain domain of S1 with respect to its catalytic domain fixed on actin, are <10%. Therefore, the ~30% changes in I_{A1} observed in these experiments are too big to be accounted for by a tilt of the lever arm and therefore must be induced by an increase in the number of myosin heads stereo-specifically bound to actin. This demonstrates that the stereo-specific "locking" of non-stereo-specifically bound myosin heads is a strain-dependent process, which is therefore accompanied by an axial "rolling" of the heads. We call this the "roll and lock" transition and assume that it is an essential part of force generation by myosin-II in muscle.

Discussion

Three New Findings Emerge from the Above-Mentioned Experiments

First, we found that the T-jump induces a biphasic change in I_{M3} (Figures 3 and 4). The fast decrease in I_{M3} begins during the 1 ms-long T-jump, i.e., on the same time scale as that following fast length steps. This fast movement of myosin heads is not accompanied by a simultaneous change in muscle force. Overall, the dip in I_{M3} resembles the dip in fiber stiffness observed after the T-jump (Bershitsky and Tsaturyan, 2002). I_{M3} changes were interpreted as a tilting of the lever arm (Irving et al., 2000). The lack of a fast change in force, in spite of a fast change in I_{M3}, suggests that part of the M3 response is associated with structural transitions in attached myosin heads, which are in pre-force-generating state(s). The contribution of detached heads to I_{M3} was shown to be negligible (Linari et al., 2000).

Second, we found that the slow phase of I_{M3}, and the increases of I_{A1} and tension after a T-jump, occur simultaneously (Figures 3 and 4). The temperature independence of steady-state fiber stiffness (Tsaturyan et al., 1999a; Bershitsky and Tsaturyan, 2002; Piazzesi et al., 2003) and the absence of changes in $I_{1,1}$ after T-jumps (Figure 3) show that temperature increases tension with a constant number of myosin heads attached to actin. Therefore, the increase in the intensities of the actin and "beating" actin-myosin layer lines after the T-jumps (Figures 1–4) is caused by a change in their mode of attachment, namely, by a transition from non-stereo-specific to stereo-specific binding. The synchronous increase in tension and in the extent of labeling of the actin helix by myosin heads shows that stereo-specific "locking" of myosin heads on actin is an intrinsic part of force generation. As previously discussed by Tsaturyan et al. (1999a), a decrease in $I_{1,0}$ at constant $I_{1,1}$ seen

after the T-jumps (Figures 3 and 4) is also characteristic of the transition from a non-stereo- to a stereo-specifically bound state.

The third finding is the strain dependence of I_{A1} (Figure 5). Its decrease after a stretch and recovery after a release suggests that the "locking" of myosin heads to a stereo-specifically bound state is accompanied by a fast force-generating "rolling" movement. These two events may either coincide, or, alternatively, the "rolling" may quickly follow a fast non-force-generating "locking." The data show that the lag between these fast and reversible events, if it exists, is less than a millisecond and takes place during phase 2 of the "Huxley-Simmons" transients. The simplest one-step "roll and lock" model is used here to account for the data, although more complicated kinetic schemes can equally account for the observations.

The next fast, reversible, and strain-dependent step can be attributed to lever arm tilting. The presence of at least two fast force-generating steps was already assumed by Huxley and Simmons (1971), as a single step could not explain quantitatively the tension transients induced by length steps. A two-step model (Piazzesi and Lombardi, 1995; Piazzesi et al., 2003) explains the mechanical transients induced by the length steps at different temperatures. The slower rise in tension and I_{A1} after T-jumps shows that there is a pool of unlocked myosin heads that are unavailable for immediate force generation. Therefore, a rate-limiting, temperature-dependent step precedes the "roll and lock" transition to account for the slow mechanical and structural responses to T-jumps and their apparent strain independence (Bershitsky and Tsaturyan, 1995, 2002).

A minimal kinetic scheme is:

$$D \leftrightarrow NA_1 \leftrightarrow NA_2 \leftrightarrow SA_1 \leftrightarrow SA_2 \rightarrow D, \qquad (1)$$

where D represents detached heads, NA_1 and NA_2 correspond to non-stereo-specifically attached heads, and SA_1 and SA_2 correspond to stereo-specifically attached states. Force developed in different states is ordered according to $0 \approx NA_1 \approx NA_2 < SA_1 < SA_2$, and axial stiffness is the same in all attached states.

The Nature of the $NA_1 \rightarrow NA_2$ Transition in Scheme 1

ATP binding to the rigor complex leads to a decrease in S1 affinity for actin, although this may not cause complete dissociation. In the presence of Ca^{2+}, dissociation of actin-S1 complexes induced by photolytic release of ATP results in a fast decay of the actin layer line structure characteristic of rigor that occurs at the same rate of >100 s^{-1} as the drop in fiber stiffness and changes in the intensities of the equatorial X-ray reflections. However, dissociation is incomplete, as the stiffness of muscle fibers and the equatorial intensities do not reach their relaxed levels, but quickly approach the values characteristic for steady-state isometric contraction that develops more slowly. As the intensity of actin-based layer lines is low, the non-force-generating heads are bound to actin non-stereo-specifically (Horiuti et al., 1997; Yagi et al., 1998; Tsaturyan et al., 1999b). Moreover, "flash and smash" EM experiments show that 20–50 ms after photolytic release of ATP in a muscle fiber in the presence of Ca^{2+}, a substantial fraction of the heads is attached to actin with a wide range of azimuthal angles and have different shapes (Hirose et al., 1993, 1994). If ATPγS (a slowly hydrolyzable ATP analog) is used instead of ATP, myosin heads do not produce tension, but they have significant instantaneous axial stiffness (Dantzig et al., 1988) and do not contribute to the actin layer lines (Kraft et al., 1999). Subsequent ATP hydrolysis, which occurs in D and in NA states, includes closing of the nucleotide pocket of S1 coupled with the return of the lever arm to the pre-power stroke orientation followed by ATP cleavage (Malnasi-Csizmadia et al., 2001; Urbanke and Wray, 2001). The return of the lever arm is fast, and a decrease in temperature shifts the equilibrium toward the open configuration of the nucleotide pocket and rigor orientation of the lever arm. The kinetics of ATP cleavage are slower than the open-close transition and significantly accelerate with temperature. Thus, acto-S1·ATP complexes in muscle fibers have mechanical and structural features similar to those expected for the NA_1 state in scheme 1, and the kinetics of ATP cleavage are also similar to that expected for the $NA_1 \rightarrow NA_2$ step.

In accordance with Dantzig et al. (1988), we consider that with ATP bound, the heads detach and reattach actin quickly. These states are non-stereo-specifically attached states. The correspondence between two-step ATP hydrolysis and scheme 1 requires that the "locking" of a myosin head on actin, i.e., the fast $NA_2 \leftrightarrow SA_1$ transition from a non-stereo-specific to a stereo-specific attachment, only occurs after ATP cleavage so that NA_2 corresponds to A·M·ADP·P_i. No experimental evidence addresses this assumption.

NA_1 in scheme 1 represents two conformations of A·M·ATP (open and closed conformations). To conform to the biochemical evidence from solution studies, we shall consider two A·M·ATP states that differ in their structure.

In contracting muscle, the transition between these structurally distinct states should produce a negative power stroke if a head remains attached to actin. The equilibrium will be different in muscle and in solution because such a negative power stroke results in storage of elastic energy. The transition is less favorable when elastic energy has to be provided. Thus, in the model below, the reverse power stroke does not occur: crossbridge detachment is required to return the myosin head to the pre-power stroke configuration.

Kinetic-Structural Model

The scheme summarizing the above-mentioned concepts is as follows:

$$\begin{array}{ccccccc} \rightarrow N_1 & & N_2 & \leftrightarrow & N_3 & \leftrightarrow S_1 \leftrightarrow S_2 \rightarrow \\ \updownarrow & & \updownarrow & & \updownarrow & & \\ D_1 & \leftrightarrow & D_2 & \leftrightarrow & D_3 & & \end{array}, \qquad (2)$$

where D_1, D_2, and D_3 represent detached heads, N_1, N_2, and N_3 correspond to non-stereo-specifically attached heads, and S_1 and S_2 correspond to stereo-specifically attached states. The scheme shown above, and the arguments presented earlier are implemented quantitatively in a model shown in Figure 6 that is used to calcu-

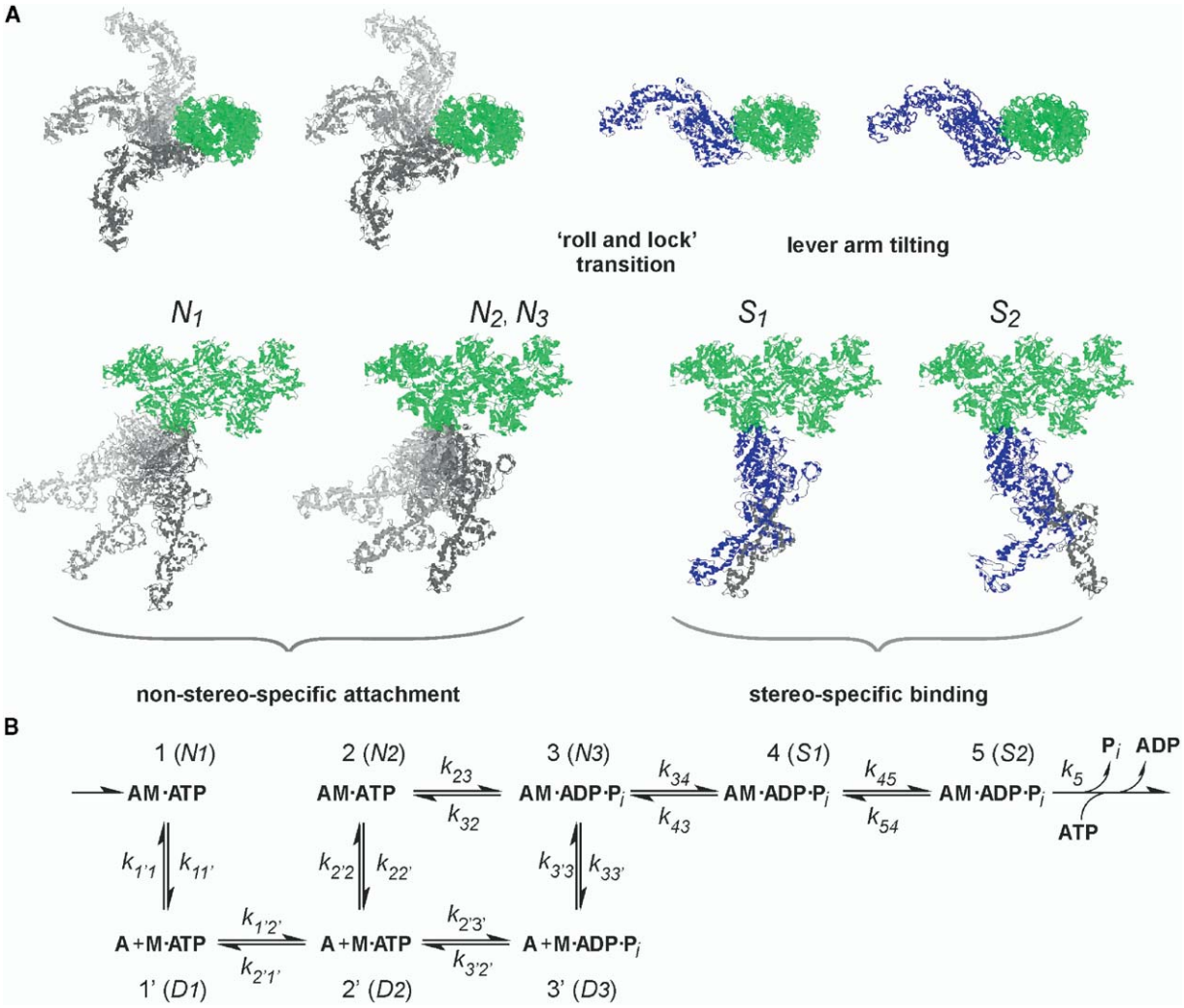

Figure 6. Kinetic and Structural Scheme of the Mechanism of Force Generation by Myosin Heads

(A) Distinct attached states in scheme 2, N_1–N_3, S_1–S_2, of a myosin head (blue or gray) bound to actin (green) are shown in two projections with the actin axis perpendicular (upper row) and parallel (lower row) to the figure plane. Labels 1–5 are used for indexing the kinetic constants. The Z-line is toward the right edge of the lower row.

(B) Kinetic scheme used in the model. Numbers without primes denote actin bound states or transitions. Prime numbers relate to actin-detached states and transitions. Pre- and post-hydrolysis states N_2 and N_3 are structurally identical, but they are biochemically different. In states N_1–N_3, the heads are axially stiff but may attach actin at different axial and azimuthal angles. The full range for azimuthal and axial angles is ±60° and ±30°, respectively. The central and extreme positions of the heads are shown in (A). Azimuthal and axial angles are randomly distributed within the full ranges. Force or displacement is produced during the "roll and lock" transition ($N_3 \rightarrow S_1$, average axial rotation of S1 as rigid body by 26°) and during the lever arm tilting ($S_1 \rightarrow S_2$, 50° axial rotation of the light chain domain with respect to the motor domain). For myosin heads in force-generating states S_1 and S_2, unstrained shapes are shown in gray and strained isometric shapes are shown in blue. In the kinetic scheme (B), M, A, ATP, ADP, and P_i are myosin S1, actin, adenosine-triphosphate, adenosine-diphosphate and inorganic phosphate, respectively. The rate constants are listed in Table 1.

late the time course of mechanical and structural changes in our experiments.

The rate constants of the kinetic steps used for the modeling are listed in Table 1. The rate constants at 5°C and 30°C for the two phases of ATP hydrolysis ($D_1 \rightarrow D_2$ and $D_2 \rightarrow D_3$ or $N_2 \rightarrow N_3$) were taken from Urbanke and Wray (2001). For simplicity, the forward and backward rate constants responsible for the "roll and lock" transition ($N_3 \rightarrow S_1$) and the lever arm tilting ($S_1 \rightarrow S_2$) were assumed to have the same temperature dependence (Table 1); thus, the equilibrium between these three states is temperature independent, while the transitions accelerate at elevated temperature, as was found for the fast tension transients following length steps in frog muscle fibers (Ford et al., 1977; Piazzesi et al., 2003). These rate constants were set in the model to account for the fast processes revealed by length steps (Figure 5). The detachment rate for non-stereo-specifically bound states, N_i, was assumed to increase with temperature to provide temperature independence of steady-state muscle stiffness (Bershitsky and Tsaturyan, 2002; Piazzesi et al., 2003). For simplicity, the same rate constants of non-stereo-specific attachment and detachment were used for all three non-stereo-specifi-

Table 1. Rate Constants for the Biochemical and Structural Transitions Used in Model Calculations

Transition	Rate Constant, s^{-1}[a]	
	5°C	30°C
1′ → 1/1 → 1′	800/1000	800/1800
2′ → 2/2 → 2′	800/1000	800/1800
3′ → 3/3 → 3′	800/1000	800/1800
1 → 2/2 → 1	0/0	0/0
2 → 3/3 → 2	50/30	1150/700
1′ → 2′/2′ → 1′	200/2000	2680/2900
2′ → 3′/3′ → 2′	50/30	1150/700
3 → 4/4 → 3	750/500	1500/1000
4 → 5/5 → 4	250/500	500/1000
5 → 1	30	60

[a] Forward/backward rate constants of the transitions between different states at 5°C and at 30°C; state numbers in the left column correspond to those in Figure 6.

cally attached states, and the rate of ATP cleavage was assumed to be the same for $D_2 \rightarrow D_3$ and $N_2 \rightarrow N_3$ (Figure 6; Table 1). The detachment-attachment rate constants of ~1000 s^{-1} were set to account for the dependence of apparent fiber stiffness on the speed of its stretch in the presence of ATP or its analogs (Dantzig et al., 1988). The generalized rate constant for product release and ATP-induced break of stereo-specific binding was set arbitrarily to match the steady-state ATPase rate. The assumption that ATP binding induces a $S_2 \rightarrow N_1$, not a $S_2 \rightarrow D_1$, transition is arbitrary and has no effect on the results of the modeling. This is because a slow transition at the end of the power stroke is followed by fast, reversible detachment-reattachment steps $N_1 \leftrightarrow D_1$. So, a new equilibrium between these non-stereo-specifically bound non-force-generating states is established very quickly.

The response of the model to a T-jump is shown in Figure 7. In a steady-state contraction at low temperature, most of the attached myosin heads are in the "open" state N_1, because the equilibrium in the "open-to-closed" transition $D_1 \leftrightarrow D_2$ is toward D_1 and ATP hydrolysis ($N_2 \rightarrow N_3$, $D_2 \rightarrow D_3$) is slow. Tension is produced by a small fraction of the heads (14.5%) in state S_i, while the total number of attached heads is ~50%. After the T-jump, the equilibrium in the "open-to-closed" transition $D_1 \leftrightarrow D_2$ shifts toward D_2, and the fraction of the heads in the "closed," pre-hydrolysis states D_2 and N_2 increases transiently. Hydrolysis also accelerates with temperature so that the post-hydrolysis states D_3 and N_3, S_1, and S_2 become more populated with some delay. A transient decrease in the number of attached heads just after the T-jump is due to acceleration of detachment from N_i states and the delay in "locking." During steady-state contraction at elevated temperature, ~65% of attached heads (or ~36% of the total number of the heads) are in force-generating, stereo-specifically bound states, while the total number of attached heads is the same as at the pre-T-jump temperature. This crossbridge state distribution is probably close to that found during isometric contraction at the physiological in vivo temperature.

The model reproduces the time course of tension, I_{A1}, and I_{M3} (Figure 3) as well as a transient decrease in fiber stiffness just after the T-jump (Figure 7), as was observed previously (Bershitsky and Tsaturyan, 2002). The increase in the fraction of stereo-specifically bound heads, S_i, closely follows ATP hydrolysis, with a time course similar to that observed for I_{A1} (Figures 3 and 4). The difference in the "cold" and "hot" levels of I_{M3} results from the axial disorder of non-stereo-specifically attached heads. The contribution of the heads in these

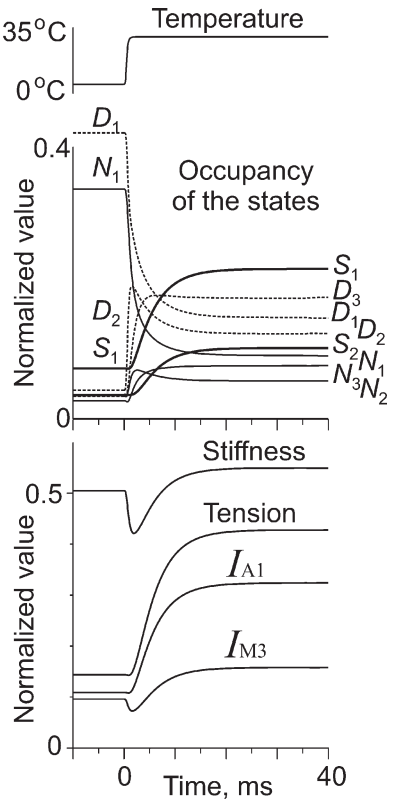

Figure 7. Modeling the Mechanical and Structural Responses to a T-Jump

From top to bottom: T-jump (from 5°C to 30°C complete in 1 ms); calculated time course of the occupancies of the attached states N_1–N_3 (continuous lines), S_1–S_2 (bold lines), and the detached states D_1–D_3 (dashed lines); fraction of attached heads (the sum of the occupancies of states N_1–N_3, S_1–S_2) approximately proportional to muscle stiffness, tension, I_{A1}, and I_{M3}. The rate constants of the transitions between the states at 5°C and 30°C are specified in Table 1; the procedure for calculating tension, I_{A1}, and I_{M3} is described in the Experimental Procedures.

states to I_{M3} is lower than that in states S_1 and S_2. Also, heads in the N_1 state are assumed to tilt as rigid bodies by 68° with respect to rigor (S_2) and so contribute less to this intensity than the more perpendicular heads in states N_2 and N_3 (Figure 6). The drop in I_{M3} just after the T-jump (Figures 3 and 4) is mainly due to a transient decrease in the fraction of bound heads (seen on the calculated stiffness trace in Figure 7) and because of the nonlinear dependence of I_{M3} on the fractions of myosin heads in the various attached states.

The two-step force generation mechanism suggested above (N_3 to S_1, S_1 to S_2) is consistent with the EM-tomography on insect flight muscles (Taylor et al., 1999) in which myosin heads in configurations similar to those assumed for attached (N_i, S_i) states of our model were observed. Namely, some heads had their light chain domains tilted at different axial and azimuthal angles compared to the catalytic domain that maintains a fixed near-rigor position on actin. Other myosin heads were attached to actin with a wide range of axial and azimuthal angles between their catalytic domains and actin. The "roll and lock" mechanism suggested here and the kinetic and structural model based on this mechanism quantitatively explain both the mechanical and the structural behavior of myosin heads in T-jump experiments and specify structural and kinetic characteristics of the two-step force generation by muscle myosin-II. An increase in I_{A1} after muscle shortening predicted by the "roll and lock" model was verified experimentally.

Experimental Procedures

Muscle Fibers and T-Jumps

Bundles of three permeabilized fibers from rabbit psoas muscle were mounted at a sarcomere length of 2.4 μm between a force transducer and a motor (Bershitsky et al., 1996). The fibers in a bundle were knotted together to improve their mechanical stability and to maintain the same sarcomere length in all fibers. In some experiments, the fibers were knotted with a hair segment of one of the authors (N.K.). Bundles were put into low-tension rigor by washing out ATP in the presence of 2,3-butanedione-monoxime (BDM) as described (Bershitsky et al., 1996) and were then partially crosslinked with 10 mM 1-ethyl-3-[3-dimethylamino)propyl]-carbodiimide (EDC) at 15°C for preserving their structural and mechanical stability, but the duration of the treatment was decreased to 5–6 min compared to 10–15 min used by Bershitsky et al. (1996, 1997) and Tsaturyan et al. (1999a). Contraction was initiated by bathing the bundle in the following solution: 100 mM 3-[N-morpholino]-propanesulfonic acid (MOPS), 5 mM MgATP, 10 mM CaEGTA, 20 mM phosphocreatine, 200 U/ml creatine phosphokinase (all chemicals from Sigma-Aldrich Co., St. Louis, MO), 5 mM dithiothreitol (DTT), ionic strength 0.15 M (pH 7.1) at 20°C. T-jumps from 5°C to ~30°C (range 28.5°C–31.5°C) were produced by passing a 1 ms long AC pulse (30 kHz, 2 kV) through the muscle sample while it was suspended in a wet, cold atmosphere (Bershitsky et al., 1997; Tsaturyan et al., 1999a; Bershitsky and Tsaturyan, 2002).

X-Ray Diffraction

Most of the experiments were carried out on the ID02 station at the European Synchrotron Radiation Facility (ESRF, Grenoble, France) by using either the FReLoN CCD detector operating at 1024 × 1024 pixel mode or the RAPID multiwire detector (Lewis et al., 1997) operating at 1024 × 1024 pixel mode. The camera length was 2.5 or 10 m. The X-ray beam at the sample was 190 or 400 μm horizontally and 245 μm vertically (FWHM). In the experiments with the RAPID detector, an aluminum strip providing ~3-fold attenuation of photon flux was placed in front of the detector in the equatorial area to prevent detector saturation by strong equatorial reflections. Experiments on beamline 16.1 at the SRS (Daresbury Laboratory, Cheshire, UK) were performed as described by Bershitsky et al. (1996). Remote control of the experiments and synchronization of the length steps and T-jumps with detector framing were already described (Bershitsky et al., 1996, 1997; Tsaturyan et al., 1999a).

Data Analysis

X-ray diffraction data were analyzed by using bsl (CCP13 suite) and BS (written by N.K., available at http://muscle.imec.msu.ru/bs_1.htm) software as described (Bershitsky et al., 1996, 1997; Koubassova and Tsaturyan, 2002). The time course of I_{M3} (Figures 3–5) was measured by integrating the total intensity in a region extending ±0.016 nm^{-1} radially and 0.0664–0.0713 nm^{-1} axially and subsequent background subtraction. Changes in I_{A1} in the T-jump experiments are obscured by reciprocal changes in the background level (Bershitsky et al., 1997; Tsaturyan et al., 1999a). The 2D intensity was integrated along the reciprocal radius in the region from 0.0269 to 0.091 nm^{-1} in each time frame at an axial spacing of 0.0175–0.0372 nm^{-1}; then, the average intensity profile before the T-jump was subtracted from those obtained in each time frame; I_{A1} for each time frame (Figure 3) was determined from this differential intensity by using xfit software (CCP13 software suite), assuming a constant position and width of the A1 peak and a variable amplitude and background level. Absolute values of I_{A1} were determined from steady-state time frames by decomposition of the A1-M1 complex (Figures 2A and 2B) into A1 and M1 peaks by using the relaxed and rigor diffraction patterns to determine the position of M1 and A1 layer lines, respectively.

Modeling

A structural-kinetic model was used for data interpretation. Differential equations for the occupancies, $c_i(t)$, of the myosin heads that populate at time t each of attached (1–5) and detached (1′–3′) states, i, in the kinetic-structural model shown in Figure 6 were integrated by the Runge-Kutta method. The rate constants at 5°C and 30°C are specified in Table 1. The T-jump duration was 1 ms. Normalized stiffness was calculated as the sum of the occupancies, $c_i(t)$, of all attached states 1–5, assuming the same stiffness for stereo-specifically and non-stereo-specifically attached states. Normalized tension was calculated as $c_4(t) + 2c_5(t)$, assuming that force produced by a myosin head in the post-power stroke state 5 is twice that in the initially "locked" state 4 and no net force is produced in the pre-force-generating states 1–3. Normalized I_{A1} was calculated as the sum of $c_4(t)$ and $c_5(t)$, assuming that a tilt of the lever arm does not affect I_{A1} (Koubassova and Tsaturyan, 2002) and neglecting any contribution from non-stereo-specifically attached heads in states 1–3. Normalized I_{M3} was calculated as the square of the amplitude of the axial Fourier transform at meridional spacing 1/14.5 nm^{-1} of the weighted sum of the electron densities of the heads in states 1–5, as shown in Figure 6. For this calculation, force-generating myosin heads in states 4 and 5 were assumed to be in their strained conformations, as shown in Figure 6, and the weight of the i-th state was equal to the fraction of the heads in this state, $c_i(t)$. I_{M3} was calculated by setting a uniform and random distribution of axial angles between S1 and actin in states N_1–N_3 (Figure 6A). A model assuming a Gaussian distribution of attachment angle was also tested. With the same SD, it gives approximately the same result as the model with uniform distribution. The contribution of detached heads to I_{M3} was neglected.

Acknowledgments

This work was supported by the Medical Research Council, the Howard Hughes Medical Institute, the International Association for the Promotion of Cooperation with Scientists from the New Independent States of the Former Soviet Union, the North Atlantic Treaty Organization, the Russian Foundation for Basic Research, the European Synchrotron Radiation Facility, the European Molecular Biology Laboratory, and the Daresbury Laboratory. Authors are very grateful to Jacques Gorini (ESRF) and Anthony Gleeson

(Daresbury Laboratory) for excellent support and to Sir Andrew Huxley and Malcolm Irving for helpful comments.

Received: June 6, 2004
Revised: November 5, 2004
Accepted: November 5, 2004
Published: January 11, 2005

References

Bershitsky, S.Y., and Tsaturyan, A.K. (1995). Force generation and work production by covalently cross-linked actin-myosin cross-bridges in rabbit muscle fibers. Biophys. J. *69*, 1011–1021.

Bershitsky, S.Y., and Tsaturyan, A.K. (2002). The elementary force generation process probed by temperature and length perturbations in muscle fibres from the rabbit. J. Physiol. *540*, 971–988.

Bershitsky, S.Y., Tsaturyan, A.K., Bershitskaya, O.N., Mashanov, G.I., Brown, P., Webb, M., and Ferenczi, M.A. (1996). Mechanical and structural properties underlying contraction of skeletal muscle fibers after partial 1-ethyl-3-[(3-dimethylamino)propyl]carbodiimide cross-linking. Biophys. J. *71*, 1462–1474.

Bershitsky, S.Y., Tsaturyan, A.K., Bershitskaya, O.N., Mashanov, G.I., Brown, P., Burns, R., and Ferenczi, M.A. (1997). Muscle force is generated by myosin heads stereospecifically attached to actin. Nature *388*, 186–190.

Bordas, J., Diakun, G.P., Diaz, F.G., Harries, J.E., Lewis, R.A., Lowy, J., Mant, G.R., Martin-Fernandez, M.L., and Towns-Andrews, E. (1993). Two-dimensional time-resolved X-ray diffraction studies of live isometrically contracting frog sartorius muscle. J. Muscle Res. Cell Motil. *14*, 311–324.

Burgess, S., Walker, M., Wang, F., Sellers, J.R., White, H.D., Knight, P.J., and Trinick, J. (2002). The prepower stroke conformation of myosin V. J. Cell Biol. *159*, 983–991.

Conibear, P.B., Bagshaw, C.R., Fajer, P.G., Kovacs, M., and Malnasi-Csizmadia, A. (2003). Myosin cleft movement and its coupling to actomyosin dissociation. Nat. Struct. Biol. *10*, 831–835.

Cope, M.J., Whisstock, J., Rayment, I., and Kendrick-Jones, J. (1996). Conservation within the myosin motor domain: implications for structure and function. Structure *4*, 969–987.

Coureux, P.D., Wells, A.L., Ménétrey, J., Yengo, C.M., Morris, C.A., Sweeney, H.L., and Houdusse, A. (2003). A structural state of the myosin V motor without bound nucleotide. Nature *425*, 419–423.

Dantzig, J.A., Walker, J.W., Trentham, D.R., and Goldman, Y.E. (1988). Relaxation of muscle fibers with adenosine 5′-[gamma-thio]triphosphate (ATP[gamma S]) and by laser photolysis of caged ATP[gamma S]: evidence for Ca2+-dependent affinity of rapidly detaching zero-force cross-bridges. Proc. Natl. Acad. Sci. USA *85*, 6716–6720.

Dobbie, I., Linari, M., Piazzesi, G., Reconditi, M., Koubassova, N., Ferenczi, M.A., Lombardi, V., and Irving, M. (1998). Elastic bending and active tilting of myosin heads during muscle contraction. Nature *396*, 383–387.

Ford, L.E., Huxley, A.F., and Simmons, R.M. (1977). Tension responses to sudden length change in stimulated frog muscle fibres near slack length. J. Physiol. *269*, 441–515.

Forkey, J.N., Quinlan, M.E., Shaw, M.A., Corrie, J.E., and Goldman, Y.E. (2003). Three-dimensional structural dynamics of myosin V by single-molecule fluorescence polarization. Nature *422*, 399–404.

Furch, M., Geeves, M.A., and Manstein, D.J. (1998). Modulation of actin affinity and actomyosin adenosine triphosphatase by charge changes in the myosin motor domain. Biochemistry *37*, 6317–6326.

Hirose, K., Lenart, T.D., Murray, J.M., Franzini-Armstrong, C., and Goldman, Y.E. (1993). Flash and smash: rapid freezing of muscle fibers activated by photolysis of caged ATP. Biophys. J. *65*, 397–408.

Hirose, K., Franzini-Armstrong, C., Goldman, Y.E., and Murray, J.M. (1994). Structural changes in muscle crossbridges accompanying force generation. J. Cell Biol. *127*, 763–778.

Holmes, K.C. (1997). The swinging lever-arm hypothesis of muscle contraction. Curr. Biol. *7*, R112–R118.

Holmes, K.C., Angert, I., Kull, F.J., Jahn, W., and Schroder, R.R. (2003). Electron cryo-microscopy shows how strong binding of myosin to actin releases nucleotide. Nature *425*, 423–427.

Horiuti, K., Yagi, N., and Takemori, S. (1997). Mechanical study of rat soleus muscle using caged ATP and X-ray diffraction: high ADP affinity of slow cross-bridges. J. Physiol. *502*, 433–447.

Houdusse, A., Kalobokis, V.N., Himmel, D., Szent-Georgyi, A.G., and Cohen, C. (1999). Atomic structure of scallop myosin subfragment S1 complexed with MgADP: a novel conformation of the myosin head. Cell *97*, 459–470.

Houdusse, A., Szent-Gyorgyi, A.G., and Cohen, C. (2000). Three conformational states of scallop myosin S1. Proc. Natl. Acad. Sci. USA *97*, 11238–11243.

Huxley, A.F. (2000). Mechanics and models of the myosin motor. Philos. Trans. R. Soc. Lond. B Biol. Sci. *355*, 433–440.

Huxley, A.F., and Simmons, R.M. (1971). Proposed mechanism of force generation in striated muscle. Nature *233*, 533–538.

Irving, M., Lombardi, V., Piazzesi, G., and Ferenczi, M.A. (1992). Myosin head movements are synchronous with the elementary force-generating process in muscle. Nature *357*, 156–158.

Irving, M., Piazzesi, G., Lucii, L., Sun, Y.-B., Harford, J.J., Dobbie, I.M., Ferenczi, M.A., Reconditi, M., and Lombardi, V. (2000). Conformation of the myosin motor during force generation in skeletal muscle. Nat. Struct. Biol. *7*, 482–485.

Joel, P.B., Trybus, K.M., and Sweeney, H.L. (2001). Two conserved lysines at the 50/20-kDa junction of myosin are necessary for triggering actin activation. J. Biol. Chem. *276*, 2998–3003.

Koubassova, N.A., and Tsaturyan, A.K. (2002). Direct modeling of X-ray diffraction pattern from skeletal muscle in rigor. Biophys. J. *83*, 1082–1097.

Kraft, T., Xu, S., Brenner, B., and Yu, L.C. (1999). The effect of thin filament activation on the attachment of weak binding cross-bridges: a two-dimensional x-ray diffraction study on single muscle fibers. Biophys. J. *76*, 1494–1513.

Kraft, T., Mattei, T., Radocaj, A., Piep, B., Nocula, C., Furch, M., and Brenner, B. (2002). Structural features of cross-bridges in isometrically contracting skeletal muscle. Biophys. J. *82*, 2536–2547.

Lewis, R.A., Helsby, W.I., Jones, A.O., Hall, C.J., Parker, B., Sheldon, J., Clifford, P., Hillen, M., Sumner, I., Fore, N.S., et al. (1997). The "RAPID" high rate large area X-ray detector system. Nucleic Instrum. Methods Phys. Res. A *392*, 32–41.

Linari, M., Piazzesi, G., Dobbie, I., Koubassova, N., Reconditi, M., Narayanan, T., Diat, O., Irving, M., and Lombardi, V. (2000). Interference fine structure and sarcomere length dependence of the axial X-ray pattern from active single muscle fibers. Proc. Natl. Acad. Sci. USA *97*, 7226–7231.

Malnasi-Csizmadia, A., Pearson, D.S., Kovacs, M., Woolley, R.J., Geeves, M.A., and Bagshaw, C.R. (2001). Kinetic resolution of a conformational transition and the ATP hydrolysis step using relaxation methods with a Dictyostelium myosin II mutant containing a single tryptophan residue. Biochemistry *40*, 12727–12737.

Piazzesi, G., and Lombardi, V. (1995). A cross-bridge model that is able to explain mechanical and energetic properties of shortening muscle. Biophys. J. *68*, 1966–1979.

Piazzesi, G., Reconditi, M., Linari, M., Lucii, L., Sun, Y.-B., Narayanan, T., Boesecke, P., Lombardi, V., and Irving, M. (2002). Mechanism of force generation by myosin heads in skeletal muscle. Nature *415*, 659–662.

Piazzesi, G., Reconditi, M., Koubassova, N., Decostre, V., Linari, M., Lucii, L., and Lombardi, V. (2003). Temperature dependence of the force-generating process in single fibres from frog skeletal muscle. J. Physiol. *549*, 93–106.

Rayment, I., Holden, H.M., Whittaker, M., Yohn, C.B., Lorenz, M., Holmes, K.C., and Milligan, R.A. (1993). Structure of the actin-myosin complex and its implications for muscle contraction. Science *261*, 58–65.

Reubold, T.F., Eschenburg, S., Becker, A., Kull, F.J., and Manstein,

D.J. (2003). A structural model for actin-induced nucleotide release in myosin. Nat. Struct. Biol. *10*, 826–830.

Smith, C.A., and Rayment, I. (1996). X-ray structure of the magnesium(II).ADP.vanadate complex of the *Dictyostelium discoideum* myosin motor domain to 1.9 Å resolution. Biochemistry *35*, 5404–5417.

Taylor, K.A., Schmitz, H., Reedy, M.C., Goldman, Y.E., Franzini-Armstrong, C., Sasaki, H., Tregear, R.T., Lucaveche, C., Edwards, R.J., et al. (1999). Tomographic 3D reconstruction of quick-frozen, Ca^{2+}-activated contracting insect flight muscle. Cell *99*, 421–431.

Tsaturyan, A.K. (2002). Diffraction by partially occupied helices. Acta Crystallogr. A *58*, 292–294.

Tsaturyan, A.K., Bershitsky, S.Y., Burns, R., and Ferenczi, M.A. (1999a). Structural changes in the actin-myosin cross-bridges associated with force generation induced by temperature jump in permeabilized frog muscle fibers. Biophys. J. *77*, 354–372.

Tsaturyan, A.K., Bershitsky, S.Y., Burns, R., He, Z.-H., and Ferenczi, M.A. (1999b). Structural responses to the photolytic release of ATP in frog muscle fibres observed by time-resolved X-ray diffraction. J. Physiol. *520*, 681–696.

Urbanke, C., and Wray, J. (2001). A fluorescence temperature-jump study of conformational transitions in myosin subfragment 1. Biochem. J. *358*, 165–173.

Volkmann, N., Ouyang, G., Trybus, K.M., DeRosier, D.J., Lowey, S., and Hanein, D. (2003). Myosin isoforms show unique conformations in the actin-bound state. Proc. Natl. Acad. Sci. USA *100*, 3227–3232.

Wong, W.W., Doyle, T.C., and Reisler, E. (1999). Nonspecific weak actomyosin interactions: relocation of charged residues in subdomain 1 of actin does not alter actomyosin function. Biochemistry *38*, 1365–1370.

Yagi, N. (1996). Labelling of thin filaments by myosin heads in contracting and rigor vertebrate skeletal muscles. Acta Crystallogr. D Biol. Crystallogr. *52*, 1169–1173.

Yagi, N., Horiuti, K., and Takemori, S. (1998). A pre-active attached state of myosin heads in rat skeletal muscles. J. Muscle Res. Cell Motil. *19*, 75–86.

Yasunaga, T., Suzuki, Y., Ohkura, R., Sutoh, K., and Wakabayashi, T. (2000). ATP-induced transconformation of myosin revealed by determining three-dimensional positions of fluorophores from fluorescence energy transfer measurements. J. Struct. Biol. *132*, 6–18.